International Journal of Fluid Mechanics Research, Vol. 32, No. 2, 2005

Combined Convection-Radiation Interaction Along a Vertical Flat Plate in a Porous Medium[†]

Harmindar S. Takhar
Department of Engineering, Manchester Metropolitan University
Manchester, M1 5GD, United Kingdom

Ali J. Chamkha
Manufacturing Engineering Department
The Public Authority for Applied Education & Training
P. O. Box 42325, Shuweikh, 70654 Kuwait

Rama Subba Reddy Gorla
Department of Mechanical Engineering, Cleveland State University
Cleveland, OH 44115, USA

An analysis is presented for the convection-radiation interaction heat transfer in boundary-layer flows over a semi-infinite flat plate with temperature dependent effective viscosity embedded in a fluid-saturated porous medium in the presence of a magnetic field. The conservation equations that govern the problem were reduced to a dimensionless form. The system was solved numerically by the Keller-box method. Asymptotic solutions for small and large values of the distance from the leading edge of the plate are presented. The influence of the various parameters entering into the problem on the velocity and heat transfer is studied.

* * *

Nomenclature

$B(x)$	magnetic field strength;
C_T	temperature difference parameter, $C_T = T_\infty/(T_W - T_\infty)$;
f	dimensionless stream function;
F	empirical constant in the second-order resistance;
G	acceleration due to gravity;
Gr	Grashof number, $\mathrm{Gr} = g\beta(T_W - T_\infty)x^3/v^3$;
Ha	Hartman number, $\mathrm{Ha} = (\sigma B_0^2/\mu)^{1/2}x$;
k	thermal conductivity;
K	permeability coefficient of the porous medium;

[†]Received 14.02.2005

ISSN 1064-2277

Nu_x Nusselt number, $Nu = hx/k$;
Pr Prandtl number, $\mathrm{Pr} = C_P \mu'_f / k$;
q_r local radiative heat flux;
q_w wall heat flux;
R conduction radiation parameter, $R = 4\sigma'(T_W - T_\infty)^3/(k\kappa^3)$;
Re_x Reynolds number, $\mathrm{Re} = u_\infty x/v$;
Ri Richardson's number, $\mathrm{Ri} = \mathrm{Gr}/\mathrm{Re}^2$;
T temperature;
u, v velocity components in x and y directions;
α thermal diffusivity;
β coefficient of thermal expansion;
η dimensionless distance;
ε porosity;
γ_f viscosity parameter, $\gamma_f = [(1/\mu')(d\mu'/dt)]_f\,(T_0 - T_\infty)$;
μ' effective viscosity of the porous medium;
ρ density;
σ electric conductivity;
σ' Stefan – Boltzmann's constant;
κ mean absorption coefficient;
γ perturbation parameter;
ψ stream function;
τ shear stress;
ϕ second order resistance, $\phi = F\varepsilon^2/\sqrt{k}$;
φ first order resistance, $\varphi = \nu\varepsilon/(ku_\infty)$;
ξ, χ dimensionless coordinates defined in Eq. (10).

Subscripts

f condition at film temperature;
w condition at the wall;
∞ condition in the free stream.

Superscripts

$'$ differentiation with respect to η.

Introduction

The study of fluid flow and heat transfer through electrically conducting porous media has received considerable interest in recent years because of the numerous applications such as magnetohydrodynamic (MHD) generators, plasma studies, nuclear reactors, oil exploration, geothermal energy extraction, and boundary layer control. The effect of a magnetic field on hydrodynamics in various configurations has been studied by Takhar and Ram [1], and Kumari [2].

It has been found in [1, 2] that in laminar boundary-layer flows over a flat plate, the presence of a solid matrix creates flow resistances, which are proportional to the velocity, and this tends to make the velocity distribution more uniform. The classical Darcy formulation is used in several studies of convection in porous media. In this model, the Darcy velocity (mean-filter velocity) $\boldsymbol{V}$ was taken

to be proportional to the pressure gradient and the gravitational force gradient. That is,

$$\boldsymbol{V} = \text{const}\frac{(\nabla p + \rho g)}{\mu}\,. \tag{1}$$

Darcy's law simulates only the bulk resistance and therefore, Brinkman [3] proposed the following equation:

$$\nabla p = \frac{\mu}{K}\boldsymbol{V} + \mu'\nabla^2\boldsymbol{V}\,, \tag{2}$$

where μ denotes the Newtonian dynamic viscosity; μ' is the effective viscosity of the porous medium; K is the permeability of the porous medium. The last term in Eq. (2) is called the Brinkman term and is similar to the diffusion term in the Navier – Stokes equations. The utility of the Brinkman equation is demonstrated by problems in which the permeability is high near the boundary. Initially, Brinkman used the following formulation for the effective viscosity: $\mu' = \mu[1 + 2.5(1 - \varepsilon_0)]$ where ε_0 is the porosity of the medium.

Kaviany [4] has shown that the interface velocity obtained from the Brinkman equation is the same as that obtained from the local simulation. Prasad and Kladias [5] emphasized that although the viscous drag term may be of relative insignificance for isothermal boundary layer flows, the vorticity diffusion has a great influence on the convective transport of energy. Owing to the presence of the microscopic shear term, the Brinkman equation exhibits full compatibility with boundary layer regions within porous media. Nield and Bejan [6] have discussed the validity of including the Brinkman term in many studies, particularly for models involving both Forscheimmer model, which works best at low porosities and the Brinkman model, which is valid at larger porosities. Evans and Plumb [7] examined the boundary layer flow past a vertical isothermal surface and concluded that for Darcy numbers $\mathrm{Da} < 10^{-7}$ ($\mathrm{Da} = K/L^2$), the viscous boundary effect was not significant. A lower rate of heat transfer was predicted when the Brinkman term was included. Sen [8] considered the Darcy – Brinkman convective flow in a shallow porous layer with adiabatic upper and lower plates and constant temperature lateral boundaries. He noted a transition in the effect of the viscous boundary effect on the Nusselt number above $\mathrm{Da} = 0.0001$, after which the heat transfer rate was seen to plummet, due to a decrease in velocity in close proximity to the wall. Vasseur and Robillard [9], Tong and Subramanian [10], and Tong and Orangi [11] studied the free convection in porous media in vertical enclosures. They observed that as the Brinkman effect increased, the heat transfer rate decreased because of the velocity decrease at the wall.

The present work has been undertaken in order to analyze the convection-radiation interaction heat transfer in boundary-layer flows over a semi-infinite flat plate with temperature-dependent effective viscosity embedded in a fluid-saturated porous medium in the presence of a magnetic field. The conservation equations that govern the problem were reduced to a dimensionless form. The system was solved numerically by the Keller-box method. Asymptotic solutions for small and large values of the distance from the leading edge of the plate have been presented. The influence of the various parameters entering into the problem on the velocity and heat transfer is studied.

1. Analysis

We consider the combined convection flow of an electrically conducting, viscous and incompressible fluid over an isothermal flat plate. The plate temperature is assumed to be T_W and that of the free stream to be T_∞. The fluid is assumed to be gray. The coordinates (x, y) are chosen such that x is measured from the leading edge of the plate and y is measured normal to the surface of the plate. The viscous dissipation and axial conduction effects are neglected. A magnetic field

strength $B(x)$ is considered to be applied normal to the plate. The effective viscosity of the porous medium μ' is assumed to depend on the temperature. Under the Boussinesq and boundary layer approximations, the conservation equations may be written as:

$$\frac{\partial u}{\partial x} + \frac{\partial v}{\partial y} = 0\,, \tag{3}$$

$$\begin{gathered} u\frac{\partial u}{\partial x} + v\frac{\partial u}{\partial y} = \frac{1}{\rho}\,\frac{\partial}{\partial y}\left(\mu'\frac{\partial u}{\partial y}\right) \\ \pm g\beta(T - T_\infty) + \frac{\sigma B^2(x)}{\rho}(u_\infty - u) + \frac{\nu\varepsilon}{K}(u_\infty - u) + \frac{F\varepsilon^2}{K^{1/2}}(u_\infty^2 - u^2), \end{gathered} \tag{4}$$

$$u\frac{\partial T}{\partial x} + v\frac{\partial T}{\partial y} = \alpha\left(\frac{\partial^2 T}{\partial y^2} - \frac{1}{k}\,\frac{\partial q_r}{\partial y}\right). \tag{5}$$

The boundary conditions are given by

$$\begin{aligned} y = 0 \quad &: \quad u = v = 0, \quad T = T_W \\ y \to \infty \quad &: \quad u = u_\infty, \qquad T = T_\infty. \end{aligned} \tag{6}$$

In the previous equations, u an v are the axial and normal velocity components, T is the temperature of the fluid in the boundary layer, g is the acceleration due to gravity, α is the thermal diffusivity, $v = \mu_f/\rho$ is the kinematic viscosity, K is the permeability, ε is the porosity, F is the empirical constant in the second-order resistance, σ is the electric conductivity, and q_r is the local radiative heat flux.

The second term on the right-hand side of Eq. (4) is the body force due to the gravitational acceleration. It should be noted that for the problem under consideration, the boundary layer will form only either when the hot surface is facing upward with $T_w > T_\infty$ or when the cold surface is facing downward with $T_w < T_\infty$.

The radiative heat flux is simplified by the Rosseland approximation [12] as:

$$q_r = -\frac{4\sigma_0}{3\kappa}\,\frac{\partial T^4}{\partial y}\,, \tag{7}$$

where σ_0 and κ are the Stefan – Boltzmann constant and the mean absorption coefficient, respectively.

For the simple case of a linear variation of viscosity with temperature, Sparrow and Cess [12], presented numerical results for a range of the viscosity variation parameter defined as:

$$\gamma_f = \left(\frac{1}{\mu'}\,\frac{d\mu'}{dT}\right)_f (T_w - T_\infty)\,, \tag{8}$$

where μ' is the effective viscosity of the medium (Brinkman-modified viscosity), and the index f refers to the conditions at film temperature of the flow $T_f = (T_w + T_\infty)/2$. Following Carey and Mollendorf [13], we assume that the absolute viscosity can be expressed as

$$\mu' = \mu'_f\left[1 + \frac{1}{\mu'_f}\left(\frac{d\mu'}{dT}\right)_f (T - T_f)\right] \tag{9}$$

where μ'_f is the value of μ' at the film temperature.

We introduce the similarity variables ξ, η with a reduced stream function $f(\xi,\eta)$ and dimensionless temperature $\theta(\xi,\eta)$ as

$$\begin{gathered}\xi = \frac{\mathrm{Gr}}{\mathrm{Re}^2}, \qquad \eta = (u_\infty \rho/\mu_f x)^{1/2} y, \\ f(\xi,\eta) = \Psi(x,y)/(\mu_f x u_\infty/\rho)^{1/2}, \qquad B(x) = B_0 x^{1/2}, \\ \theta(\xi,\eta) = \begin{cases} (T-T_\infty)/(T_w-T_\infty) & \text{for hot surface,} \\ (T-T_w)/(T_\infty-T_w) & \text{for cold surface,} \end{cases}\end{gathered} \tag{10}$$

where $\mathrm{Gr} = g\beta(T_w - T_\infty)x^3/v^2$ and $\mathrm{Re} = u_\infty x/\nu$ are the local Grashof and Reynolds numbers.

When the transformations given by Eq. (10) are applied to Eqs (4) and (5), the governing system of equations becomes

$$\begin{gathered}\left[1+\gamma_f\left(\theta-\frac{1}{2}\right)\right]f''' + \left(\frac{1}{2}f+\gamma_f\theta'\right)f'' + \frac{\mathrm{Gr}}{\mathrm{Re}^2}\xi\theta + \frac{\mathrm{Ha}^2}{\mathrm{Re}}\xi(1-f') \\ +\varphi\xi(1-f') + \phi\xi(1-f'^2) = \xi\left[f'\frac{\partial f'}{\partial\xi} - f''\frac{\partial f}{\partial\xi}\right],\end{gathered} \tag{11}$$

$$\theta''\left[1+\frac{4R}{3}(C_T+\theta)^3\right] + 4R(C_T+\theta)^2\theta'^2 + \frac{1}{2}\mathrm{Pr}f\theta' = \xi\mathrm{Pr}\left[f'\frac{\partial\theta}{\partial\xi} - \theta'\frac{\partial f}{\partial\xi}\right]. \tag{12}$$

The boundary conditions are given by:

$$f(\xi,0) = f'(\xi,0) = 0, \qquad \theta(\xi,0) = 1, \qquad f'(\xi,\infty) = 1, \qquad \theta(\xi,\infty) = 0. \tag{13}$$

2. Solution

2.1. Numerical Solution by Keller-Box Method. The governing equations of the problem under investigation are solved numerically by the Keller-box method which is an implicit scheme with unconditional stability. The method allows for nonuniform grid discretization and converts the differential equations into algebraic ones which are then solved by a Thomas algorithm. We have used 301 grid points in the ξ direction and 196 grid points in the η direction. Variable step sizes in the η direction with an initial step size of 0.001 and a growth factor of 1.03 and constant step sizes of 0.01 in the ξ direction are employed. A mesh sensitivity exercise has been performed to ensure grid independence. The solution convergence criterion required that the difference between current and previous iteration be 10^{-5}.

2.2. Asymptotic Solution with ξ as a small parameter. Here we use a series of expressions to solve (11), (12). We treat ξ as a small parameter so that we get the combined effects of forced and free convection on the flow near the leading edge. The Asymptotic expansion of f and θ in ξ may be assumed to be

$$\begin{aligned} f(\xi,\eta) &= \sum_{j=0}^{\infty}\xi^j f_j(\eta) = f_0(\eta) + \xi f_1(\eta) + \xi^2 f_2(\eta) + \cdots, \\ \theta(\xi,\eta) &= \sum_{j=0}^{\infty}\xi^j \theta_j(\eta) = \theta_0(\eta) + \xi\theta_1(\eta) + \xi^2\theta_2(\eta) + \cdots \end{aligned} \tag{14}$$

By substituting expressions in Eq. (14) into Eqs (11) and (12) and equating like powers of ξ, we obtain series solution valid for small values of ξ. These details are documented by Mansour and Gorla [14].

2.3. Asymptotic Solution with ξ as a large parameter.

Outer layer. We now set the main layer equations (11) and (12) the following expansion:

$$f(\xi,\eta) = F_0(\eta) + \xi^{-1/2}F_1(\eta) + \cdots, \tag{15}$$

$$\theta(\xi,\eta) = \Theta_0(\eta) + \xi^{-1/2}\Theta_1(\eta) + \cdots, \tag{16}$$

Equating the coefficients for ξ^0 and $\xi^{-1/2}$, we have we have:

$$F_0'''\left(1+\gamma_f\left(\Theta_0-\frac{1}{2}\right)\right) + F_0''\left(\frac{1}{2}F_0+\gamma_f\Theta_0'\right) - F_1'^2\phi = 0, \tag{17}$$

$$F_1'''\left(1+\gamma_f\left(\Theta_0-\frac{1}{2}\right)\right) + F_0'''\Theta_1\gamma_f + \left[F_0''\gamma_f\Theta_1' + \frac{1}{2}F_1''F_0 + F_1''\gamma_f\Theta_0' + \frac{1}{2}F_1'F_0'\right] = 0, \tag{18}$$

$$\Theta_0''\left[1+\frac{4R}{3}(C_T+\Theta_0)^3\right] + 4R(C_T+\Theta_0)^2\Theta_0'^2 + \frac{1}{2}\mathrm{Pr}F_0\Theta_0' = 0, \tag{19}$$

$$\begin{gathered}\Theta_1''\left[1+\frac{4R}{3}(C_T+\Theta_0)^3\right] + 4R\Theta_1(C_T+\Theta_0)^2 \\ +8R[(C_T+\Theta_0)\Theta_1\Theta_0'^2 + (C_T+\Theta_0)^2(\Theta_0'\Theta_1') + \mathrm{Pr}\Theta_1'F_0 = 0,\end{gathered} \tag{20}$$

Eqs (17) – (20) were solved numerically using the fourth-order Runge – Kutta scheme.

Inner layer. We now set the inner layer equations (11) and (12) the following expansion:

$$\chi = \eta\xi, \tag{21}$$

$$f(\xi,\chi) = \xi^{-2}F_0(\chi) + \xi^{-5/2}F_1(\chi) + \cdots, \tag{22}$$

$$\theta(\xi,\chi) = 1 + \xi^{-1/2}\Theta_0(\chi) + \xi^{-1}\Theta_1(\chi) + \cdots \tag{23}$$

Substituting Eqs (21) – (23) into Eqs (11) and (12) and equating coefficients of ξ^{-2} and $\xi^{-5/2}$ we get:

$$\left(F_0''' + \frac{1}{2}F_0'''\gamma_f\right) + \gamma_f F_0'' = 0, \tag{24}$$

$$F_1''' + F_0'''\gamma_f\Theta_0 + \frac{1}{2}F_1'''\gamma_f + \gamma_f F_0''\Theta_0' + \gamma_f F_1'' = 0, \tag{25}$$

$$8R(C_T+1)^2\Theta_0' + \Theta_0''(C_T+1)^3 + 3(C_T+1)^2\Theta_0 + 8R(C_T+1)\Theta_0 = 0, \tag{26}$$

$$\Theta_1''\left(C_T+1\right)^3+3\left(C_T+1\right)^2\Theta_1+3\left(C_T+1\right)\Theta_0^2$$
$$+8R\left[\left(C_T+1\right)^2\left(\Theta_1'+\frac{1}{2}{\Theta_0'}^2\right)+\left(C_T+1\right)\Theta_1+\frac{1}{2}\Theta_0^2\right]=0. \tag{27}$$

The boundary conditions are given by

$$\begin{aligned}\chi=0 \quad &: \quad F_0=F_0'=F_1=F_1'=0,\Theta_0=1, \qquad \Theta_1=0,\\ \chi=\infty \quad &: \quad F_0=F_1=0,F_0'=1,F_1'=0, \qquad \Theta_0=\Theta_1=0.\end{aligned} \tag{28}$$

Solution for the inner layer equations is given by

$$F_0=\frac{F_0(0)(2+\gamma_f)}{4\gamma_f}\left[-2+2e^{\frac{-2\gamma_f}{2+\gamma_f}\chi}+\left(-1+e^{\frac{-2\gamma_f}{2+\gamma_f}\chi}+2\chi\right)\gamma_f\right], \tag{29}$$

$$\begin{aligned}-F_1=&\Bigg\{\Theta_0'(C_T+1)e^{(m+p)\chi}F_0(0)(-1+m^2+mn)(m-p)\\ &-\frac{1}{m+n}(m+p)^2(-1+m^2+mp)\Theta_0'(0)(C_T+1)e^{(m+p)\chi}F_0(0)\\ &+2(-1+m^2+mn)\big(m^3-p+2m^2p+m(-1+p^2)\big)\\ &\times\chi\big(-\Theta_0'(0)(C_T+1)F_0(0)p+am(m+p)F_1(0)\big)\\ &+\frac{1}{m+n}\big[(-1+m^2+mn)(-1+m^2+mp)\big(-\Theta_0'(C_T+1)F_0(0)\big(2m^3p+p(n+p)\\ &+2m^2p(n+p)+m(3p+n(-1+2p^2))\big)+2am^2(m+n)(m+p)^2F_1(0)\big)\big]\\ &+\frac{1}{(1+m)n}2e^{m\chi}m^2\Bigg[\Theta_0'(C_T+1)F_0(0)\big[m^5p+n(-0.5n-0.5p)p^2+2m^4p(n+p)\\ &+mp\big(-1.5np-0.5p^2+n^2(-1+p^2)\big)+m^3\big(-0.5p+n^2p+p^3+n(-0.5+4p^2)\big)\\ &+m^2\big(-p^2+n^2(-0.5+2p^2)+n(-1.5p+2p^3)\big)\big]\\ &-a(m^3-n+2m^2n+m(-1+n^2))(m+p)^2(-1+m^2+mp)F_1(0)\Bigg]\Bigg\}\\ &\times\frac{1}{2a(-1+m^2+mn)(m+p)^2(-1+m^2+mp)},\end{aligned} \tag{30}$$

where

$$a=\sqrt{-3(C_T+1)-8R+16R^2},$$

$$m=-\frac{2\gamma_f}{2+\gamma_f} \qquad n=\frac{-4R+a}{C_T+1}, \qquad p=-\frac{4R+a}{C_T+1} \tag{31}$$

$$\Theta_0=-\frac{1}{a}\Theta_0'(0)(C_T+1)\left(e^{\frac{-4R-a}{C_T+1}\chi}-e^{\frac{-4R+a}{C_T+1}\chi}\right),$$

$$\Theta_1 = \Bigg\{(C_T+1)e^{\frac{a-4R}{C_T+1}\chi}\Big[3a^3\Theta_1'(0)+4a^2R\big(\Theta_1'(0)-2(\Theta_0'(0))^2(C_T+1)\big)$$

$$-48aR^2\Theta_1'(0)-64R^3\Theta_1'(0)+2(\Theta_0'(0))^2(C_T+1)\big(3(C_T+1)+4R+64R^3\big)\Big]\Bigg\}$$

$$\times\frac{1}{2a(a-4R)(a+4R)(3a+4R)}$$

$$+\Bigg\{(C_T+1)e^{\frac{-a-4R}{C_T+1}\chi}\Big[-3a^3\Theta_1'(0)+4a^2R\big(\Theta_1'(0)-2(\Theta_0'(0))^2(C_T+1)\big)$$

$$+48aR^2\Theta_1'(0)-64R^3\Theta_1'(0)+2(\Theta_0'(0))^2(C_T+1)\big(3(C_T+1)+4R+64R^3\big)\Big]\Bigg\}$$

$$\times\frac{1}{2a(a+4R)(3a^2-16aR+16R^2)} \tag{32}$$

$$-\Bigg\{(\Theta_0'(0))^2(C_T+1)^2e^{\frac{-2(a+4R)}{C_T+1}\chi}\Big[24a^4\big(1-6e^{\frac{2a}{C_T+1}\chi}+e^{\frac{4a}{C_T+1}\chi}\big)R$$

$$-64a^3\big(-1+e^{\frac{4a}{C_T+1}\chi}\big)R^2+16a\big(-1+e^{\frac{4a}{C_T+1}\chi}\big)R\big(3(C_T+1)+4R+64R^3\big)$$

$$+16\big(-1+e^{\frac{2a}{C_T+1}\chi}\big)^2R^2\big(3(C_T+1)+4(R+32R^3)\big)$$

$$+a^2\big[9(C_T+1)\big(1+6e^{\frac{2a}{C_T+1}\chi}+e^{\frac{4a}{C_T+1}\chi}\big)$$

$$-4R\big(-3+128R^2+e^{\frac{4a}{C_T+1}\chi}(-3+128R^2)-2e^{\frac{2a}{C_T+1}\chi}(9+320R^2)\big)\big]\Big]\Bigg\}$$

$$\times\frac{1}{4a^2(9a^4-160a^2R^2+256R^4)}\,.$$

3. Results and Discussion

The numerical results of the present analysis are obtained for the case of hot surface. The velocity and temperature profiles for the case of hot surface are plotted in figures for varying values of R, γ_f, C_T, Ha, Ri, φ and ϕ.

The velocity and temperature distributions within the boundary layer for all cases studied are not shown in the paper in order to save space. As R increases, the velocity and temperature within the boundary layer increase. Figs 1 and 2 show that the surface friction factor increases with R whereas the surface heat transfer rate decreases as R increases. As the viscosity gradient parameterγ_f increases, the velocity diminishes whereas the temperature increases. As seen from Figs 3 and 4, the friction factor and surface heat transfer rate decrease as the viscosity gradient parameter γ_f increases. As the temperature difference parameter C_T increases, the velocity and temperature fields get augmented. As seen from Figs 5 and 6, the friction factor increases and surface heat transfer rate decreases as temperature difference parameter C_T increases. As the Hartmann number Ha increases, the velocity and temperature fields get reduced. As seen from Figs 7

and 8, the friction factor increases and surface heat transfer rate decreases as Ha increases. As the Richardson number Ri increases, the velocity increases and temperature reduces. For Ri grater than one, we notice that the velocity profile has a local maximum greater than the free stream velocity. As seen from Figs 9 and 10, the friction factor and surface heat transfer rate increase as Ri increases. The velocity and temperature profiles are relatively insensitive to the parameter φ. As seen from Figs 11 and 12, the friction factor and surface heat transfer rate increase as parameter φ increases. As the parameter ϕ increases, the velocity increases and temperature decreases. As seen from Figs 13 and 14, the friction factor and surface heat transfer rate increase as parameter ϕ increases.

Concluding Remarks

In this paper, we have presented a boundary layer analysis for flow of fluid over a semi-infinite plate with temperature-dependent effective viscosity in a porous medium in the presence of magnetic field. The governing equations are transformed into a set of nonlinear ordinary differential equations, where a numerical solution has been presented for a wide range of parameters. An asymptotic solution is presented for large distances from the leading edge of the plate. The numerical results indicated that the buoyancy increases heat transfer from the surface. The effect of the magnetic field is to reduce the surface heat transfer. This can have some applications of cooling by applying a magnetic field at the surface.

REFERENCES

1. Vafai, K. and Tien,, Boundary and Inertia Effects on Flow and Heat Transfer in Porous Media, *Int. J. Heat Mass Transfer*, 1981, **24**, pp. 195–203.
2. Vafai, K., Connective Flow and Heat Transfer in Variable Porosity Media, *J. Fluid Mech.*, 1984, **147**, pp. 233–259.
3. Brinkman, H. C., A Calculation of the Viscous Forces Exerted by a Flowing Fluid on a Dense Swarm of Particles, *Appl. Sci. Resch*, 1947, **47**, pp. 27–34.
4. Kaviany, M., *Principles of Heat Transfer in Porous Media*, New York, McGraw Hill, 1991.
5. Prasad, V. and Kladias, N., Non Darcy Natural Convection in Saturated Porous Media, In: *Convective Heat and Mass Transfer in Porous Media*, Kluwer Academic, NATO Series in Applied Science, Dordrecht, 1991.
6. Nield, D. A. and Bejan, A., *Convection in Porous Media*, Springer Verlag, New York, 1992.
7. Evans, G. H and Plumb, O. A. Natural Convection from a Vertical Isothermal Surface Embedded in a Saturated Porous Medium In: *AIAA/ASME Thermophys. and Heat Transfer Conf.*, Palo Alto, California, 1978, Pap. No. 78-HT-55.
8. Sen, A. K., Natural Convection in a Shallow Porous Cavity: The Brinkman Model, *Int. J. Heat Mass Transfer*, 1987, **30**, pp. 855–868.
9. Vasseur, P. and Robillard, L., The Brinkman Model for Boundary Layer Regime in a Rectangular Cavity with Uniform Heat Flux from the Side, *Int. J. Heat Mass Transfer*, 1987, **30**, pp. 717–728.
10. Tong, T. W. and Subramanian, E., A Boundary Layer Analysis for Natural Convection in Vertical Porous Enclosures: Use of Brinkman Extended Darcy Model, *Int. J. Heat Mass Transfer*, 1985, **28**, pp. 563–571.

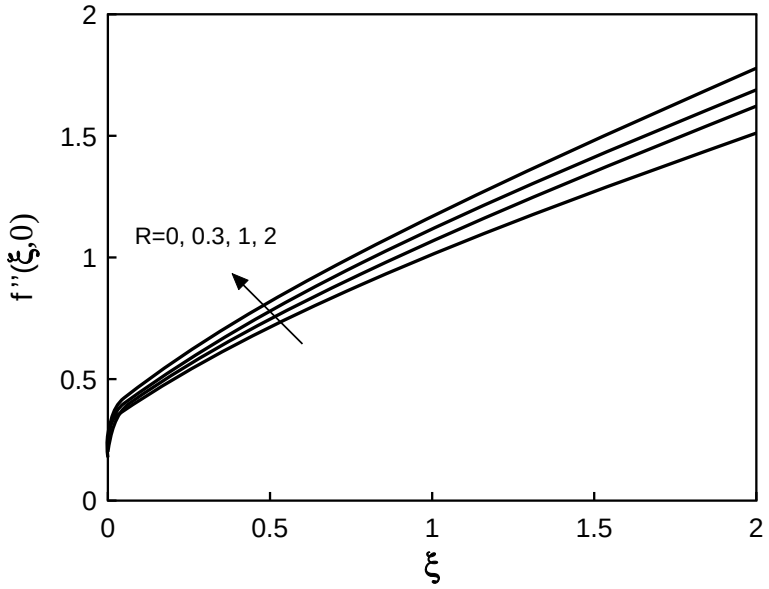

Fig. 1. Effects of R on local wall shear stress:
$C_T = 0.1$, $\mathrm{Ha} = 0$, $\mathrm{Pr} = 0.71$, $\mathrm{Ri} = 1$, $\phi = 0$, $\gamma_f = 0.8$, $\varphi = 0$.

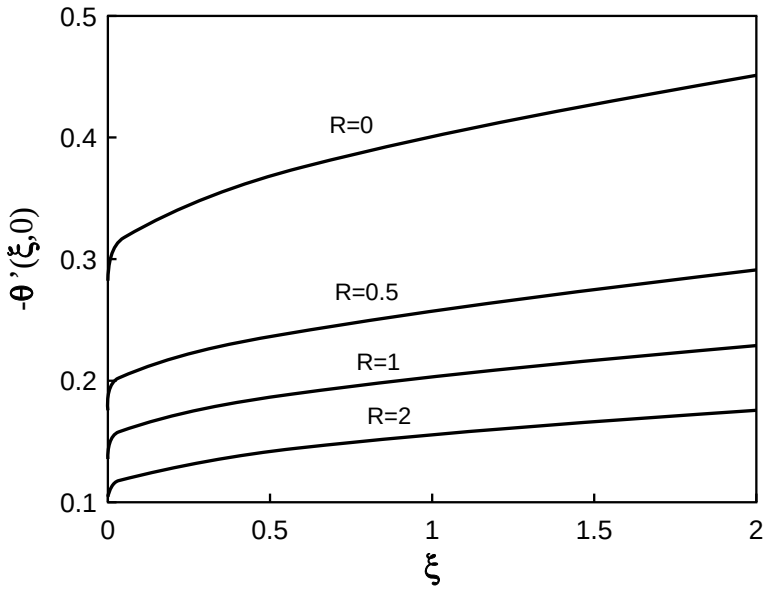

Fig. 2. Effects of R on local wall heat flux:
$C_T = 0.1$, $\mathrm{Ha} = 0$, $\mathrm{Pr} = 0.71$, $\mathrm{Ri} = 1$, $\phi = 0$, $\gamma_f = 0.8$, $\varphi = 0$.

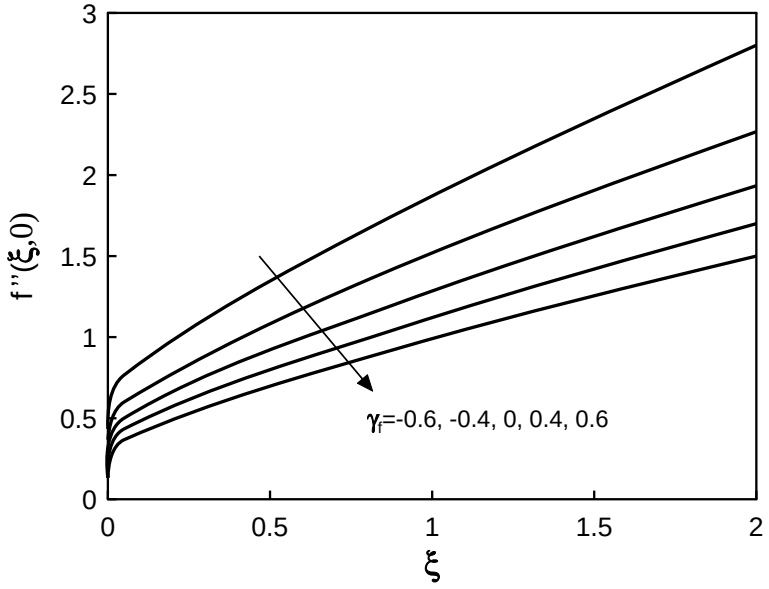

Fig. 3. Effects of γ_f on local wall shear stress:
$C_T = 0.1$, $\mathrm{Ha} = 0$, $\mathrm{Pr} = 0.71$, $R = 0$, $\mathrm{Ri} = 1$, $\phi = 0$, $\varphi = 0$.

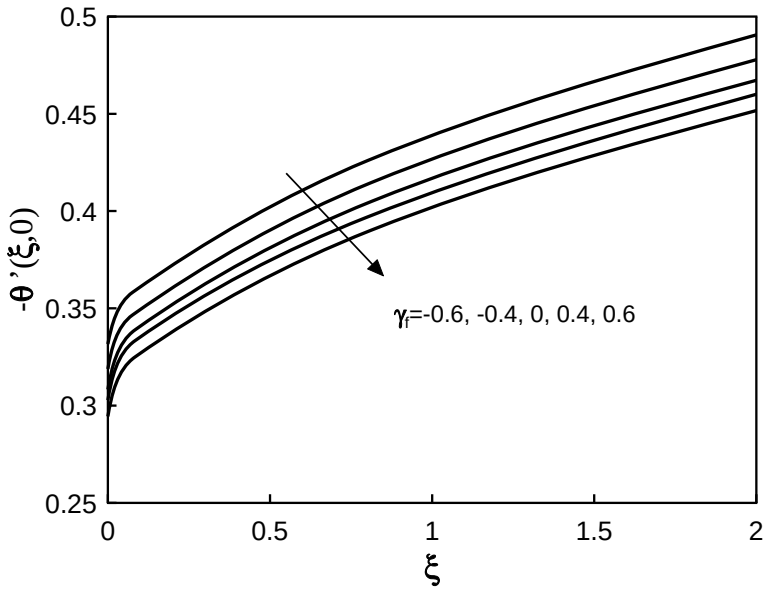

Fig. 4. Effects of γ_f on local wall heat flux:
$C_T = 0.1$, $\mathrm{Ha} = 0$, $\mathrm{Pr} = 0.71$, $R = 0$, $\mathrm{Ri} = 1$, $\phi = 0$, $\varphi = 0$.

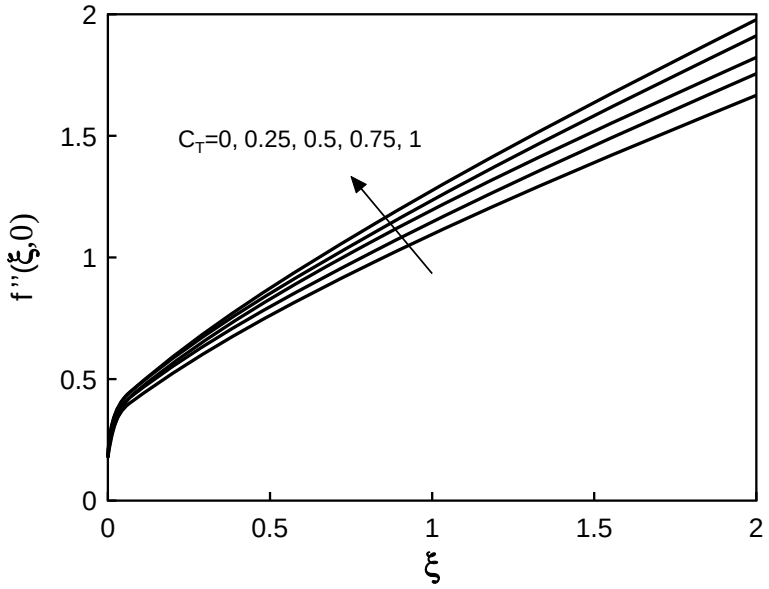

Fig. 5. Effects of C_T on local wall shear stress:
$\mathrm{Ha} = 0$, $\mathrm{Pr} = 0.71$, $R = 0$, $\mathrm{Ri} = 1$, $\phi = 0$, $\gamma_f = 0.8$, $\varphi = 0$.

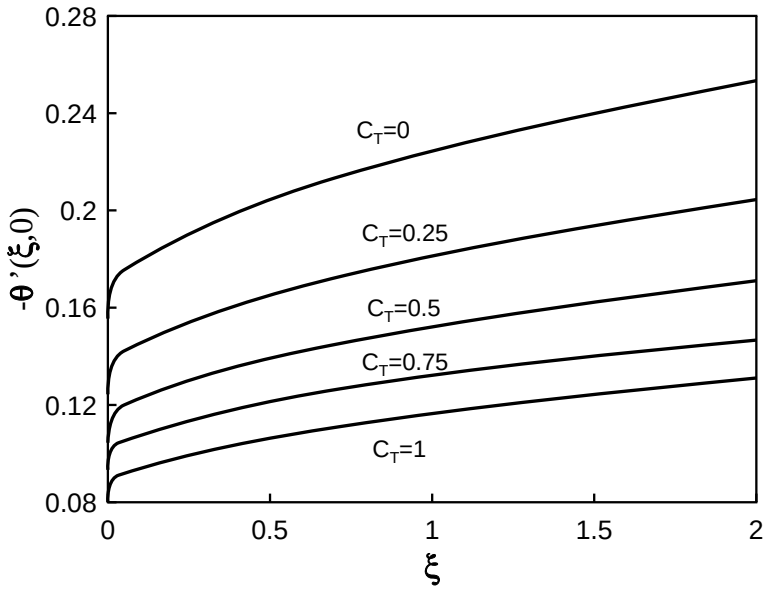

Fig. 6. Effects of C_T on local wall heat flux:
$\mathrm{Ha} = 0$, $\mathrm{Pr} = 0.71$, $R = 0$, $\mathrm{Ri} = 1$, $\phi = 0$, $\gamma_f = 0.8$, $\varphi = 0$.

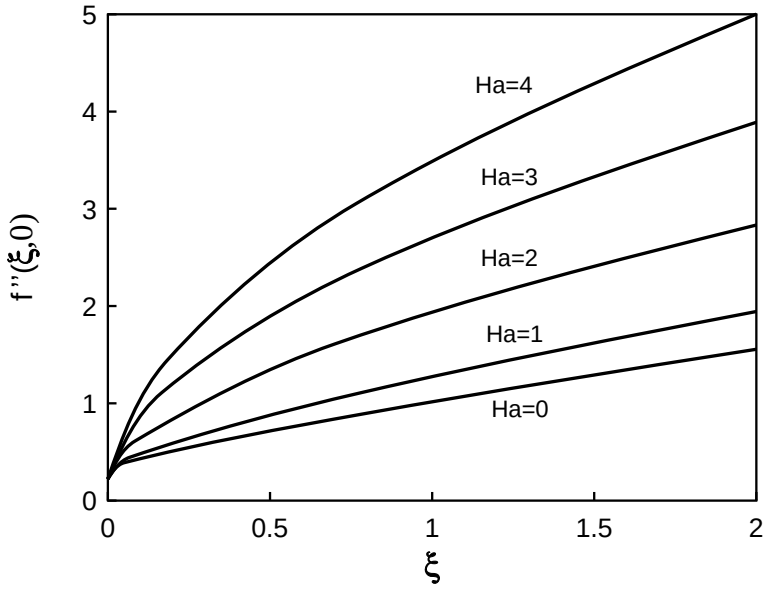

Fig. 7. Effects of Ha on local wall shear stress:
$C_T = 0.1$, $\mathrm{Pr} = 0.71$, $R = 0$, $\mathrm{Ri} = 1$, $\phi = 0$, $\gamma_f = 0.8$, $\varphi = 0$.

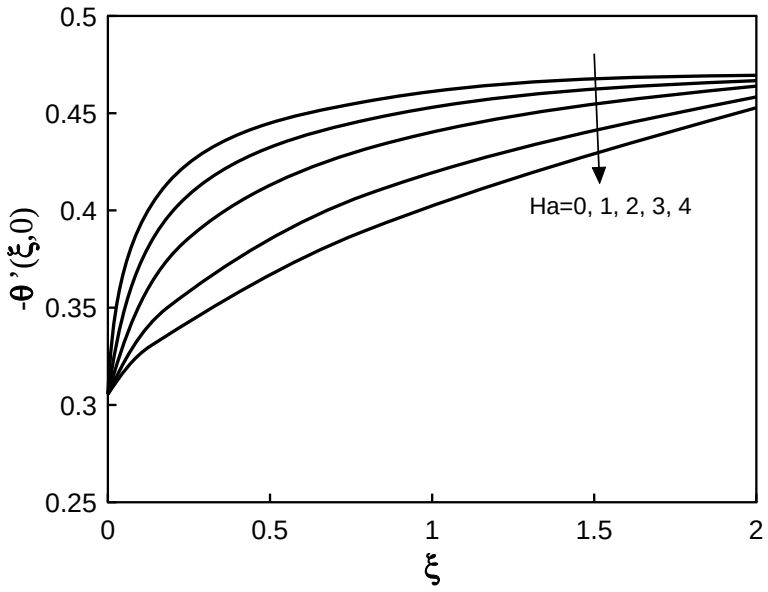

Fig. 8. Effects of Ha on local wall heat flux:
$C_T = 0.1$, $\mathrm{Pr} = 0.71$, $R = 0$, $\mathrm{Ri} = 1$, $\phi = 0$, $\gamma_f = 0.8$, $\varphi = 0$.

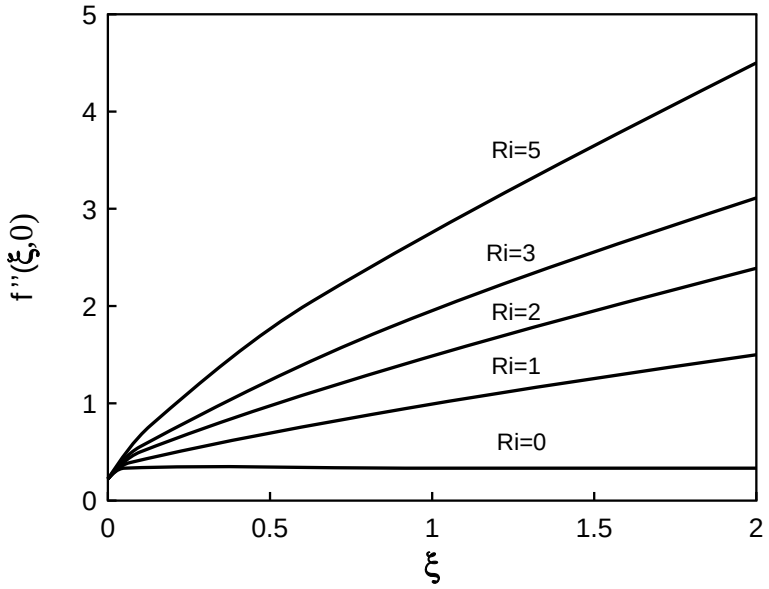

Fig. 9. Effects of Ri on local wall shear stress:
$C_T = 0.1$, Ha $= 0$, Pr $= 0.71$, $R = 0$, $\phi = 0$, $\gamma_f = 0.8$, $\varphi = 0$.

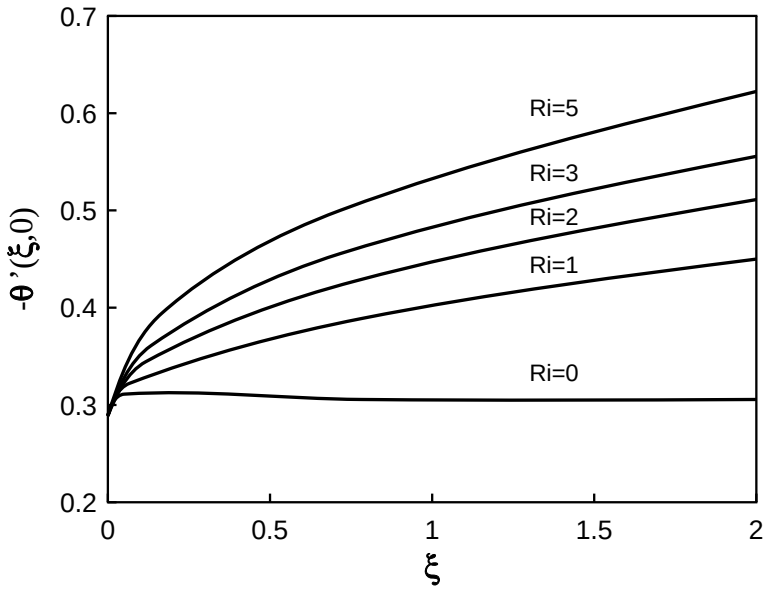

Fig. 10. Effects of Ri on local wall heat flux:
$C_T = 0.1$, Ha $= 0$, Pr $= 0.71$, $R = 0$, $\phi = 0$, $\gamma_f = 0.8$, $\varphi = 0$.

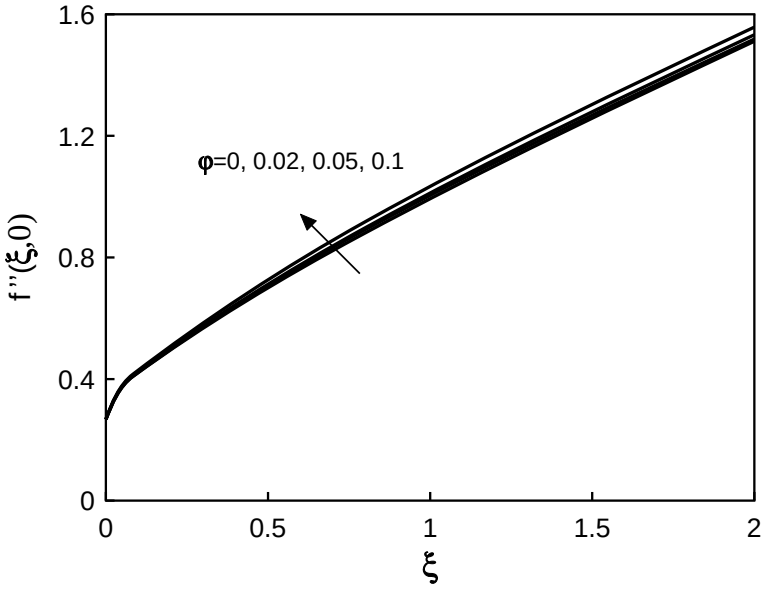

Fig. 11. Effects of φ on local wall shear stress:
$C_T = 0.1$, $\mathrm{Ha} = 0$, $\mathrm{Pr} = 0.71$, $R = 0$, $\mathrm{Ri} = 1$, $\phi = 0$, $\gamma_f = 0.8$.

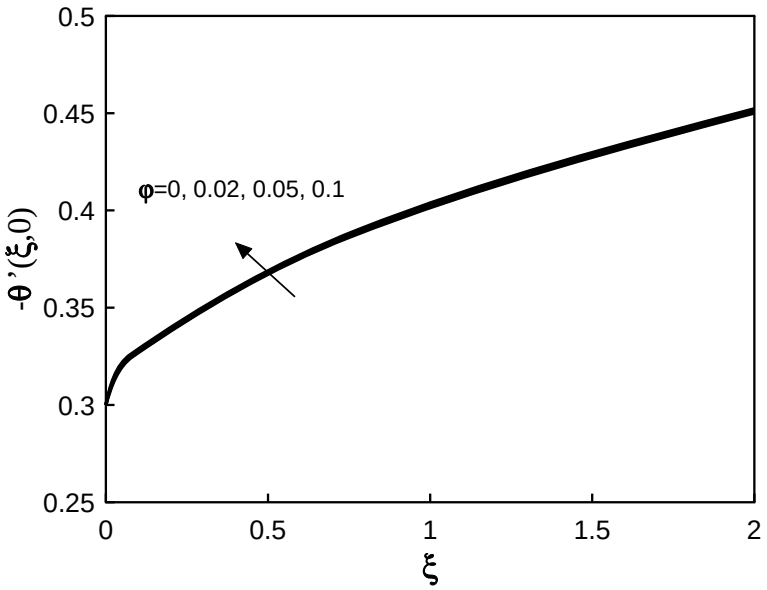

Fig. 12. Effects of φ on local wall heat flux:
$C_T = 0.1$, $\mathrm{Ha} = 0$, $\mathrm{Pr} = 0.71$, $R = 0$, $\mathrm{Ri} = 1$, $\phi = 0$, $\gamma_f = 0.8$.

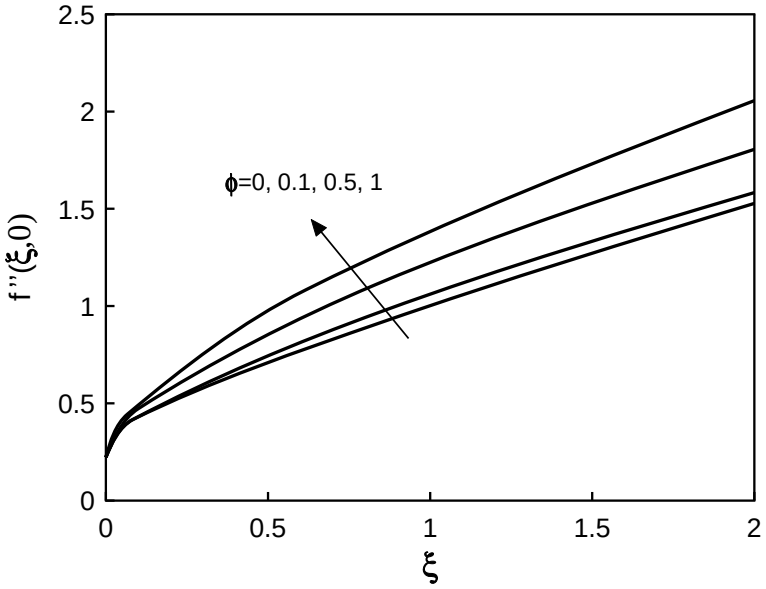

Fig. 13. Effects of ϕ on local wall shear stress:
$C_T = 0.1$, $\mathrm{Ha} = 0$, $\mathrm{Pr} = 0.71$, $R = 0$, $\mathrm{Ri} = 1$, $\gamma_f = 0.8$, $\varphi = 0.02$.

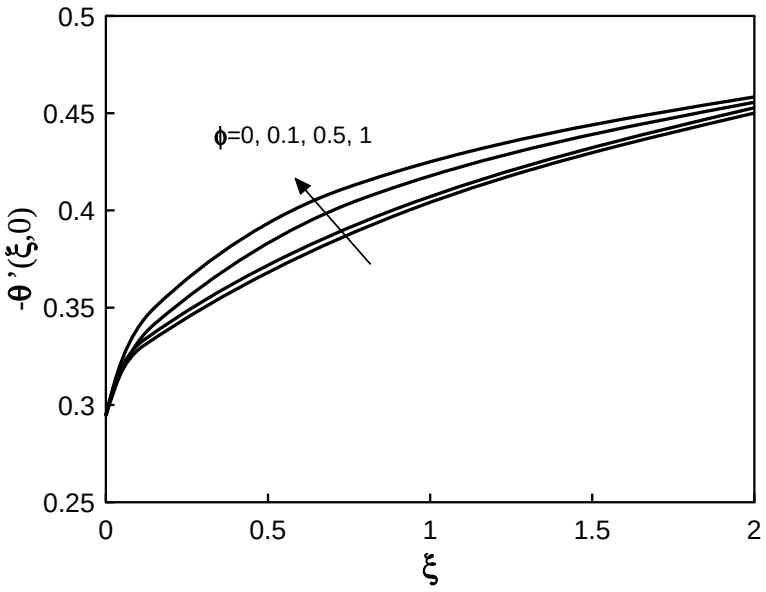

Fig. 14. Effects of ϕ on local wall heat flux:
$C_T = 0.1$, $\mathrm{Ha} = 0$, $\mathrm{Pr} = 0.71$, $R = 0$, $\mathrm{Ri} = 1$, $\gamma_f = 0.8$, $\varphi = 0.02$.

Table 1
Values of $F_0(0)$, $\Theta_0'(0)$, $F_1(0)$ and $\Theta_1'(0)$ are obtained after keeping
$\Pr = 0.71$, $\gamma_f = 0.8$, $C_T = 0.1$, $\phi = 0$ as constant and applying various values of R.

R	Pr	γ_f	C_T	ϕ	$F_0(0)$	$\Theta_0'(0)$	$F_1(0)$	$\Theta_1'(0)$
0	0.71	0.8	0.1	0	0.23825	−0.27842	0.05321	0.14285
0.5	0.71	0.8	0.1	0	0.24604	−0.17789	0.05795	0.09211
1	0.71	0.8	0.1	0	0.24791	−0.13881	0.06321	0.07495
1.5	0.71	0.8	0.1	0	0.25232	−0.11905	0.06882	0.06364
2	0.71	0.8	0.1	0	0.25772	−0.10601	0.06902	0.05719

Table 2
Values of $F_0(0)$, $\Theta_0'(0)$, $F_1(0)$ and $\Theta_1'(0)$ are obtained after keeping
$R = 1.0$, $\Pr = 0.71$, $C_T = 0.1$, $\phi = 0$ as constant and applying various values of γ_f.

R	Pr	γ_f	C_T	ϕ	$F_0(0)$	$\Theta_0'(0)$	$F_1(0)$	$\Theta_1'(0)$
1	0.71	−0.8	0.1	0	0.50408	−0.15836	0.04521	0.08851
1	0.71	−0.4	0.1	0	0.39998	−0.15238	0.04521	0.08278
1	0.71	0	0.1	0	0.33345	−0.14675	0.04421	0.08034
1	0.71	0.4	0.1	0	0.28805	−0.14315	0.05421	0.07759
1	0.71	0.8	0.1	0	0.24791	−0.13881	0.06321	0.07495

Table 3
Values of $F_0(0)$, $\Theta_0'(0)$, $F_1(0)$ and $\Theta_1'(0)$ are obtained after keeping
$R = 1.0$, $\Pr = 0.71$, $\gamma_f = 0.8$, $\phi = 0$ as constant and applying various values of C_T.

R	Pr	γ_f	C_T	ϕ	$F_0(0)$	$\Theta_0'(0)$	$F_1(0)$	$\Theta_1'(0)$
1	0.71	0.8	0	0	0.24712	−0.15261	0.06821	0.07985
1	0.71	0.8	0.25	0	0.25387	−0.12453	0.06821	0.06654
1	0.71	0.8	0.5	0	0.26087	−0.10633	0.04633	0.05791
1	0.71	0.8	0.75	0	0.26209	−0.09232	0.05251	0.05274
1	0.71	0.8	1	0	0.26709	−0.08252	0.05151	0.04812

Table 4
Values of $F_0(0)$, $\Theta_0'(0)$, $F_1(0)$ and $\Theta_1'(0)$ are obtained after keeping
$R = 1.0$, $\gamma_f = 0.8$, $\Pr = 0.71$, $C_T = 0.1$ as constant and applying various values of ϕ.

R	Pr	γ_f	C_T	ϕ	$F_0(0)$	$\Theta_0'(0)$	$F_1(0)$	$\Theta_1'(0)$
1	0.71	0.8	0.1	0	0.24791	−0.13881	0.06321	0.07495
1	0.71	0.8	0.1	0.02	0.24781	−0.13861	0.06221	0.07485
1	0.71	0.8	0.1	0.05	0.24751	−0.13846	0.05781	0.07488
1	0.71	0.8	0.1	0.1	0.24665	−0.13839	0.05645	0.07401
1	0.71	0.8	0.1	0.5	0.24304	−0.13829	0.05599	0.07321

11. Tong, T. W. and Orangi, S., A Numerical Analysis for High Modified Rayleigh Number Natural Convection in Enclosures Containing a Porous Medium, *Heat Transfer*, 1986, **5**, pp. 2647–2652.
12. Sparrow, E. M. and Cess, R. D., *Radiation Heat Transfer Augmented Edition*, Hemisphere, Washington, 1978, Chaps 7 and 10.
13. Carey, V. P. and Mollendorf, J. C., Natural Convection in Liquids with Temperature Dependent Viscosity, In: *Proc 6th Int. Heat Transfer Conf. Toronto*, Vol. 2, Hemisphere, Washington, 1978, pp. 211–217.
14. Mansour, M. A. and Gorla, R. S. R., MHD Mixed Convection-Radiation Interaction Along a Vertical Flat Plate in a Porous Medium, *J. MHD Plasma Resch*, 2000, **9**, pp. 197–228.

□◆◆◆□